ChemPlusChem

Research Article
doi.org/10.1002/cplu.202300378

Chemistry Europe
European Chemical Societies Publishing

www.chempluschem.org

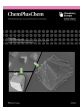

Direct Electrochemical Synthesis of Metal-Organic Frameworks: $Cu_3(BTC)_2$ and Cu(TCPP) on Copper Thin films and Copper-Based Microstructures

Ana María Araújo-Cordero,[a, b] Francesco Caddeo,[a, c] Behzad Mahmoudi,[a] Michael Bron,[b] and A. Wouter Maijenburg*[a]

Cu thin films and Cu_2O microstructures were partially converted to the Metal-Organic Frameworks (MOFs) $Cu_3(BTC)_2$ or Cu(TCPP) using an electrochemical process with a higher control and at milder conditions compared to the traditional solvothermal MOF synthesis. Initially, either a Cu thin film was sputtered, or different kinds of Cu or Cu_2O microstructures were electrochemically deposited onto a conductive ITO glass substrate. Then, these Cu thin films or Cu-based microstructures were subsequently coated with a thin layer of either $Cu_3(BTC)_2$ or Cu(TCPP) by controlled anodic dissolution of the Cu-based substrate at room temperature and in the presence of the desired organic linker molecules: 1,3,5-benzenetricarboxylic acid (BTC) or photoactive 4,4′,4″,4‴-(Porphine-5,10,15,20-tetrayl) tetrakis(benzoic acid) (TCPP) in the electrolyte. An increase in size of the Cu micro cubes with exposed planes [100] of 38,7% for the $Cu_2O@Cu_3(BTC)_2$ and a 68,9% increase for the Cu_2O@Cu(TCPP) was roughly estimated. Finally, XRD, Raman spectroscopy and UV–vis absorption spectroscopy were used to characterize the initial Cu films or Cu-based microstructures, and the obtained core-shell $Cu_2O@Cu(BTC)$ and Cu_2O@Cu(TCPP) microstructures.

Introduction

Metal–Organic Frameworks (MOFs) are porous materials with open crystalline structures accessible to other molecules or atoms, giving them the highest specific surface area known until now.[1] First published by Li et al. in 1999,[2] MOFs have crystalline structures as frameworks, where metal ions or metal oxide nodes are directly linked by organic bridging molecules.[1] One of the most exciting features in their synthesis is the possibility of selecting or exchanging their building units (metallic nodes or organic linkers) according to the desired physicochemical properties, making these hybrid materials highly tailorable, unique and versatile.[3] This feature extends the chemical functionalization of MOFs, brings adaptability and versatility to their crystalline structure, and increases their potential use,[4] which includes the storage and separation of gases, sensors, catalysis, functional materials,[5–11] and as templates for the deposition of nanoparticles.[12,13]

Normally, MOFs are crystallized via a spontaneous self-assembly process of their components by solvothermal reactions, but this method provides little control over the shape and size of the produced powder material.[1] However, the synthesis of both MOF thin films and MOF microstructures is an essential and promising field, because they can produce MOFs in direct contact with the substrate rather than their deposition as a powder, allowing superior performance in advanced applications, including chemical sensors, membranes and photoelectrodes.[3,4,14] The controlled MOF synthesis as continuous and conformal films is an emerging field that makes use of several strategies, such as liquid-phase epitaxy,[15] Langmuir–Blodgett layer-by-layer deposition,[16] seeded growth,[17] in-situ growth[14] and electrochemical deposition.[18–30] The Electrochemical MOF (EMOF)[31] film growth was reported for the first time by Mueller et al.[32] and has crucial advantages as process technique, such as a direct contact between the MOF and the substrate, a relatively simple procedure with few reaction steps at mild conditions, and precise control of the process variables.[23,29] Several MOFs have been synthesized using electrochemical methods, such as anodic electrodeposition, cathodic electrodeposition and electrophoretic deposition, including $Cu_3(BTC)_2$, Cu(BDC), $Cu(INA)_2$, MOF-5 and MIL-

[a] A. M. Araújo-Cordero, Dr. F. Caddeo, B. Mahmoudi, Prof. A. Wouter Maijenburg
Center for Innovation Competence SiLi-nano
Martin-Luther-Universität Halle-Wittenberg
Karl-Freiherr-von-Fritsch-Straße 3
06120 Halle (Germany)
E-mail: wouter.maijenburg@chemie.uni-halle.de

[b] A. M. Araújo-Cordero, Prof. M. Bron
Institut für Chemie
Technische Chemie
Martin-Luther-Universität Halle-Wittenberg
Von-Danckelmann-Platz 4
06120 Halle (Germany)

[c] Dr. F. Caddeo
Institute for Nanostructures and Solid State Physics
University of Hamburg
Luruper Chaussee 149, Bld. 600, Room 2.59
22761 Hamburg (Germany)

Supporting information for this article is available on the WWW under https://doi.org/10.1002/cplu.202300378

100.[22,25,33] During an anodic EMOF film growth, the metallic atoms on the electrode surface are oxidized to form cations (nodes), which react with deprotonated linkers in the electrolyte, directly forming the desired MOF crystals, and avoiding possible contaminations and intermediate layers.[34]

EMOF synthesis has a wide range of parameters depending of the desired product. For example, the first electrochemically produced $Cu_3(BTC)_2$ was synthesized as a loose powder in the electrolyte using a wide applied potential range between 12 and 19 V vs. a Cu counter electrode for 150 minutes, as reported by Mueller et al.[32] Electrochemically synthesized MOF films were directly synthesized on Cu foil substrates by applying a potential range between 1 and 30 V vs. a Cu counter electrode, as reported by Van de Voorde et al.[20] The synthesis conditions reported by Caddeo et al.[35] consist of an applied potential of 2.5 V vs. a Cu counter electrode as the oxidation voltage to convert Cu nanostructures into $Cu_3(BTC)_2$ and $Cu(INA)_2$. This last work was taken as a reference for the experiments in this research.

In addition to the clear advantages of producing new MOF materials as thin films, an increase in the development of nano- or microstructures with well-defined geometry (e.g. solid and hollow spheres, prisms, rods, wires and dendrites) has been reported in recent decades as a promising strategy to overcome the trade-off between a relatively lower amount of active sites of the catalytic material and a higher surface area per unit volume, resulting in an enhancement of its catalytic and physicochemical properties in this size regime.[36–48]

Furthermore, MOF-containing core-shell micro- and nanostructures have been proposed as multi-functional materials, with applications ranging from drug delivery platforms based on biocompatible MOFs[49] to enhanced supercapacitors[50,51] and electrocatalysts,[50] including engineered size-selective catalysts by the modulation of the pore aperture size of the MOF shell.[52,53]

Despite the mentioned advantages, only a few MOFs have been synthesized as thin films or microstructures, especially when compared to the wide variety of reported MOF powders, and even fewer have been synthesized on transparent electrodes such as ITO.[34] The synthesis of both MOF thin films and microstructures with high crystallinity, orientation and controllable thickness, their characterization by standard and non-sample-destructive methods, and their direct application after synthesis are still current challenges, because many MOFs with desirable chemical functionalities are difficult or impossible to achieve directly.[52,54]

Understanding the possibility of a wide range of applications and the desirability of developing core-shell MOF microstructures, we selected a wide range of Cu-based microstructures (i.e. Cu_2O cubes, Cu_2O octahedra, Cu dendrites and Cu_2O dendritic microstructures) as a proof of concept for the controlled MOF conversion, aiming to produce core-shell microstructures. Furthermore, this research focuses on the preparation of either $Cu_3(BTC)_2$ or Cu(TCPP) MOF coatings from two different Cu-based substrates: Cu thin films and Cu-based microstructures with a defined geometry, which were the only Cu source in the MOF synthesis.

Both substrates, the Cu thin films and the selected Cu-based microstructures, were directly deposited on conductive ITO glass and were used as electrodes. The developed MOF synthesis is a pulsed electrochemical oxidation process for the direct conversion of the Cu thin films and Cu-based microstructures at room temperature and with milder conditions compared to traditional solvothermal MOF synthesis reactions. This process allows the use of 70 nm thin Cu films as the substrate, which is a thinner Cu film compared to the substrates used by Ji et al.,[14] and Cu-based cubes, rhombohedra and dendrites, achieving homogeneous EMOF synthesis of either $Cu_3(BTC)_2$ or Cu(TCPP) via anodic dissolution using a three electrodes electrochemical setup with a saturated Ag/AgCl reference electrode.

To the best of our knowledge, this is the first time that an electrochemical synthesis of Cu(TCPP) has been successfully achieved on both Cu thin films and Cu_2O microstructures.[14,22,25,26,31,33,35,54–58]

Results and Discussion

In preliminary experiments, it was observed that both $Cu_3(BTC)_2$ and Cu(TCPP) crystallized when the Cu thin film substrates were simply immersed in the corresponding electrolyte solutions at room temperature, i.e. 25 °C, without an applied bias (supporting information, Figure S.1 and S.2a). For better control by electrochemical synthesis and a higher quality of the obtained MOF films, the four parameters that play an important role during the MOF conversion were tuned, so that the desired MOF (either $Cu_3(BTC)_2$ or Cu(TCPP)) only crystallizes when a bias potential was applied, and not by simple immersion. First, the amount of ethanol in the solution was changed from 50% v/v to 75% v/v compared to the reported method by Caddeo et al.,[35] which resulted in a reduction of the diffusion of Cu ions from the substrate surface,[14,59] increasing the concentration of Cu ions in the vicinity of the Cu thin film substrate, and thereby increasing the density of MOF crystals (Supporting information, Figure S.2b). Second, tributylmethylammonium methyl sulfate (MTBS) was not used in the solution, which also resulted in a reduction of the diffusion of Cu ions from the substrate surface (Supporting information, Figure S.2c). Third, all the MOF conversion reactions were done at 25 °C, compared to the 55 °C reported by Caddeo et al.,[35] which also reduces the diffusion of Cu ions from the substrate and facilitates the milder synthesis conditions. Finally, Triethylamine (TEA) was added into the solution, which deprotonated the selected organic linker and hindered the MOF crystallization on the Cu thin film surface without applied potential (Figure S.3).[14]

As reported by Ji et al.,[14] the concentration of TEA to be added into the electrolyte depends on the number of protons of the selected carboxylic acid, i.e. if the carboxylic acid is BTC with three protons, the concentration of TEA should be 17.4 mM, corresponding to three times 5.8 mM as the concentration of BTC. For TCPP, the electrolyte contained 5.8 mM TCPP and 23.2 mM TEA. Once TEA was used as additive to the solution, the pH of the electrolyte changed for both organic

linker (BTC: from 4.11 to 8,00. TCPP: from 3.9 to 8.10) and the Cu thin film samples did not present mayor changes after one hour of immersion, allowing the control of the Cu-based MOF synthesis just via electrochemical oxidation (Supporting information, Figure S.3).

In this research, another important variable in the electrochemical synthesis of Cu-based MOFs is the selection of either a constant or a pulsed oxidation potential. For comparison, two Cu thin films were treated with either a constant applied potential of 2 V vs. $Ag/AgCl_{(sat)}$ for 60 s or a pulsed potential of 2 V vs. $Ag/AgCl_{(sat)}$ for 0.5 s with a resting potential of 0 V vs. $Ag/AgCl_{(sat)}$ for 0.5 s, which was repeated 120 times, resulting in a total deposition time of 60 s. In the case of the pulsed experiment, the number of cycles was chosen so that the total oxidation time was the same as that of the samples prepared under continuous bias. The current density during the electrochemical oxidation is comparable for both, as shown in the chronoamperograms displayed in the Supporting information, Figure S.4a. It is important to mention that additionally, the applied potential was reduced to 2 V compared to the 2.5 V reported by Caddeo et al.[35] This reduction of the applied potential was possible, because the thin films are completely exposed to the electrolyte, while the substrates reported by Caddeo et al. were nanostructures in a template with a lower surface exposed to the electrolyte. In general, a lower oxidation potential is preferred for the thin films to control the MOF formation, as shown in the supporting information, Figure S.5a–b.

As shown in Figure S.5a–b, all Cu film samples changed color and texture from polished metallic rose to a more opaque surface after the EMOF film growth in the BTC-containing electrolyte. On the other hand, the samples exposed to the TCPP-containing electrolyte showed less evident changes (Supporting information, Figure S.5c). The EMOF film growth was homogeneous over the whole surface exposed to the electrolyte when it was examined with the naked eye. The Cu thin film substrates have a reduced detachment after the $Cu_3(BTC)_2$ pulsed electrochemical conversion compared to the constant applied bias in the area in contact with the sample holder (see Supporting Information, Figure S.5a and S.5b). The same pulsed oxidation procedure also worked perfectly for the Cu(TCPP) MOF, for which no detachment from the electrode's surface was observed after conversion (Figure S.5c). In Figure 1, SEM images of a) a bare Cu thin film, b) the obtained $Cu_3(BTC)_2$ crystals and c) the obtained Cu (TCPP) film via our optimized pulsed electrochemical oxidation process are shown. In the deposited $Cu_3(BTC)_2$ film shown in b), individual crystals are displayed with the characteristic and well-known octahedral shape of this MOF,[14,23,24,27,30,60–63] as it is also shown in the supporting information, Figure S.6. Additionally, cross-section SEM images of the $Cu_3(BTC)_2$ were used to measure the thickness of the produced coating with an obtained range between 32.5 nm and 229.2 nm, as shown in the Supporting Information Figures S.7a) and b). On the other hand, in Figure 1c), it can be observed that the Cu(TCPP) film was composed of more compact and interconnected crystals, resulting in the synthesis of a continuous MOF film, especially when compared to the more individual and isolated $Cu_3(BTC)_2$ crystals, as also shown in the supporting information, Figure S.6. This lamellar crystalline array of the Cu(TCPP) film is typical for this MOF, as it was also observed and reported by La et al. using wet chemistry as the synthesis method,[58] and by Rahimi et al. using a solvothermal reaction.[57] For this MOF, also cross-section SEM images were used to measure the thickness of the produced coating with an obtained range between 45.1 nm and 212.4 nm, as shown in the supporting information Figures S.7c) and d).

The obtained MOF-coated films were also characterized by XRD and Raman spectroscopy, as shown in Figure 2a) and 2b), respectively. The XRD peaks of $Cu_3(BTC)_2$ marked with an asterisk (*) on top of the green curve in Figure 2a) are at the same position as the calculated diffraction pattern by Morita et al.,[35] confirming the successful deposition of $Cu_3(BTC)_2$. Unfortunately, the Cu(TCPP) film after electrochemical oxidation did not present any additional peaks compared to the bare Cu film.

Conversely, Raman spectroscopy was used as a structural fingerprint, due to its lower penetration depth into the sample, making it possible to analyze the surface of the substrates.[66–69] Both prepared MOF thin films, $Cu_3(BTC)_2$ (green curve in Figure 2b) and Cu(TCPP) (blue curve in Figure 2b) presented similar Raman spectra as reported samples synthesized with other methods. The Raman peaks of the $Cu_3(BTC)_2$ marked with an asterisk are in agreement with those reported by Schäfer et al.[21] and by Todaro et al.[70] for a powder $Cu_3(BTC)_2$ sample,[70] while the Cu(TCPP) peaks marked with a plus sign (+) are at the same position as reported by Sun et al. for a powder Cu(TCPP) sample.[71] It is important to highlight that the Raman peak

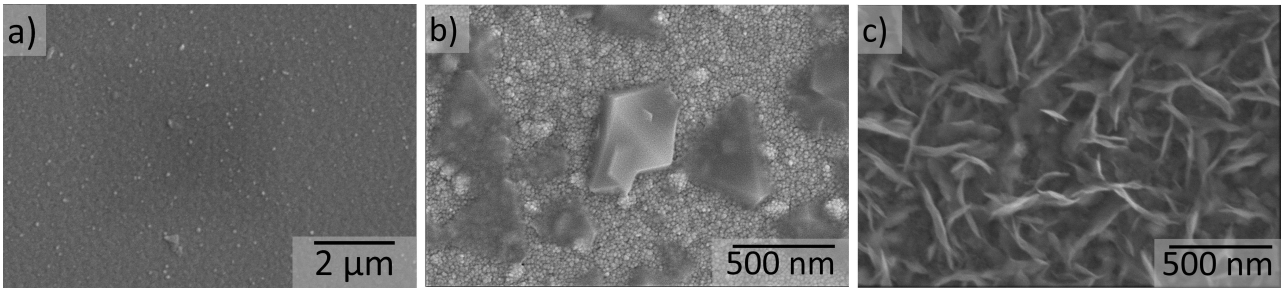

Figure 1. SEM images obtained of a) a bare Cu thin film substrate, b) a $Cu_3(BTC)_2$ and c) a Cu(TCPP) film synthesized electrochemically via anodic dissolution by applying a pulsed potential of 2 V for 0.5 s and a potential of 0 V for 0.5 s for 120 times with a total oxidation time of 60 s.

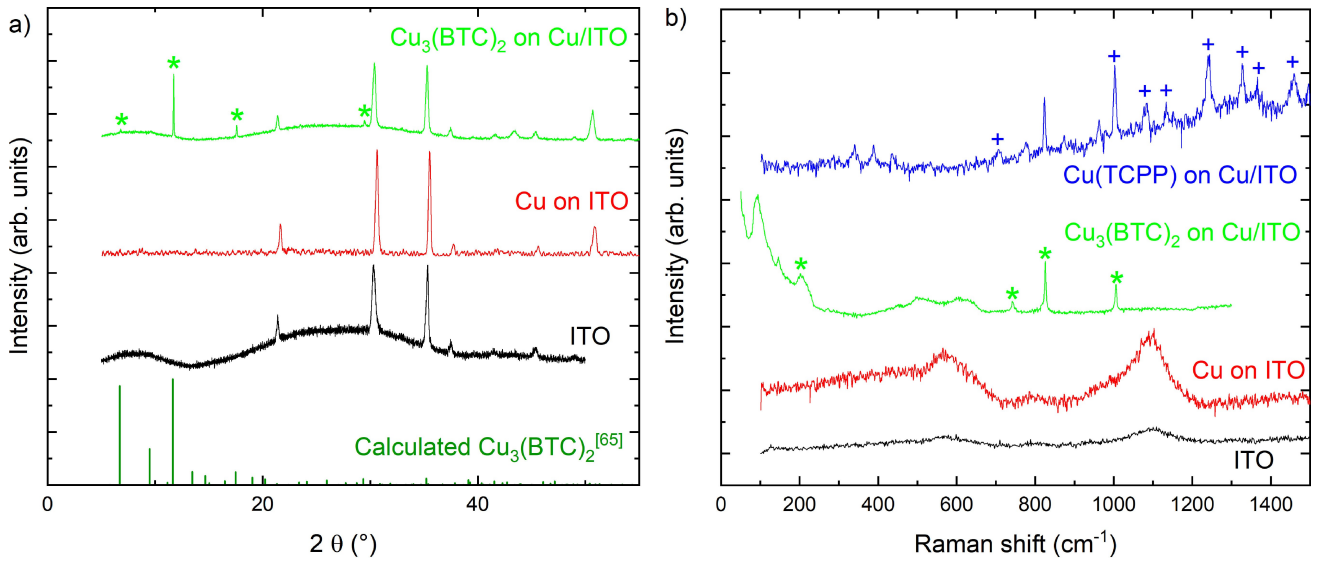

Figure 2. a) XRD and b) Raman spectra obtained from ITO (black curves), a bare Cu thin film on ITO (red curves), and $Cu_3(BTC)_2$ films on Cu/ITO (green curves) and a Cu(TCPP) film on Cu/ITO (blue curve) obtained via pulsed electrochemical conversion at 25 °C. The calculated XRD pattern for $Cu_3(BTC)_2$ is displayed in dark green near the x axis and the corresponding peaks were marked with an asterisk (*) on top of the green curve in a). This calculated XRD pattern was obtained from the Cambridge Crystallographic Data Centre[64] with the identifier FUNGAZ by Morita et al.[65]

located at 825 cm^{-1} is characteristic of the MOF $Cu_3(BTC)_2$, so it is not shared with the organic linker (BTC).[21]

To extend the presented approach to other substrates and for a proof of principle, the same electrochemical MOF synthesis was applied for the synthesis of core-shell microstructures. For this, three different types of either Cu or Cu_2O microstructures (i.e. microcubes, octahedra and dendrites) were selected to compare the effect of the crystal shape on the Cu-based MOF conversion (i.e. $Cu_3(BTC)_2$ and Cu(TCPP)). After their synthesis by electrodeposition, the Cu or Cu_2O microstructures were converted into core-shell hybrid microstructures using the presented pulsed electrochemical anodic dissolution to achieve a controlled synthesis of either $Cu_3(BTC)_2$ or Cu(TCPP) coatings under milder conditions compared to more traditional solvothermal MOF synthesis methods. Again, the selected microstructures were used as the only source of Cu for this synthesis.[72] During this process, the appearance of the sample (color and texture) did not change when examined at first sight, but the change of color of the microstructures before and after the MOF conversion was more evident when investigated with an optical microscope (Supporting information, Figures S.8 and S.9). While the dendritic Cu microstructures completely covered the surface exposed to the electrolyte, the density of the Cu_2O crystals on the ITO electrodes was considerably different between the cubic Cu_2O microstructures with exposed [100] crystallographic planes and octahedral Cu_2O microstructures with exposed [111] crystallographic planes before the MOF conversion (Supporting information, Figure S.8 and S.10). This difference in the amount of Cu_2O crystals on the ITO substrate has a major influence on the performed characterization of the samples, as is shown in the obtained UV–vis spectra in the supporting information (Figure S.16). However, it was not possible to achieve or improve to a more homogeneous distribution of the microstructures under the studied conditions.

A partial electrochemical conversion from these Cu or Cu_2O microstructures into core-shell Cu@Cu-based MOF or Cu_2O@Cu-based MOF microstructures was aimed so that any improvement of the core-shell microstructures due to the MOF coating can be studied and directly compared with bare Cu or Cu_2O microstructures. Additionally, the application of a pulsed potential (with two steps) allows a controlled and homogeneous oxidation of the Cu_2O microstructures, avoiding the complete detachment of these microstructures from the ITO glass, as may occur when applying a constant oxidation potential, as was evidenced when using Cu thin films as a substrate (supporting information, Figure S.5). Finally, a pulsed electrochemical conversion allows the formation of a conformal MOF coating on the microstructure surface by a continuous renewal of the concentration of the organic linker (either BTC or TCPP) during application of the resting potential.

SEM analysis was used to examine the Cu_2O microstructures before and after pulsed electrochemical oxidation in an electrolyte containing BTC or TCPP linker molecules, as shown in Figure 3. It was observed that the Cu_2O cubes (Figure 3a, 3b and 3c), octahedra (Figure 3d, 3e and 3f) and dendrites (Figure 3g, 3h, 3i and 3j) have a defined geometrical shape that remains more or less the same after the electrochemical oxidation process. Additionally, all samples presented changes on their surface after the electrochemical MOF conversion into $Cu_3(BTC)_2$ or Cu(TCPP), as shown in Figure 3 and in the supporting information, Figure S.11. The cubic Cu_2O microstructures show a less prominent change on their surface, whereas the octahedra and dendrite samples show a significant change on their surface, which is due to the inherent thermodynamic stability, characteristic of each microstructure.

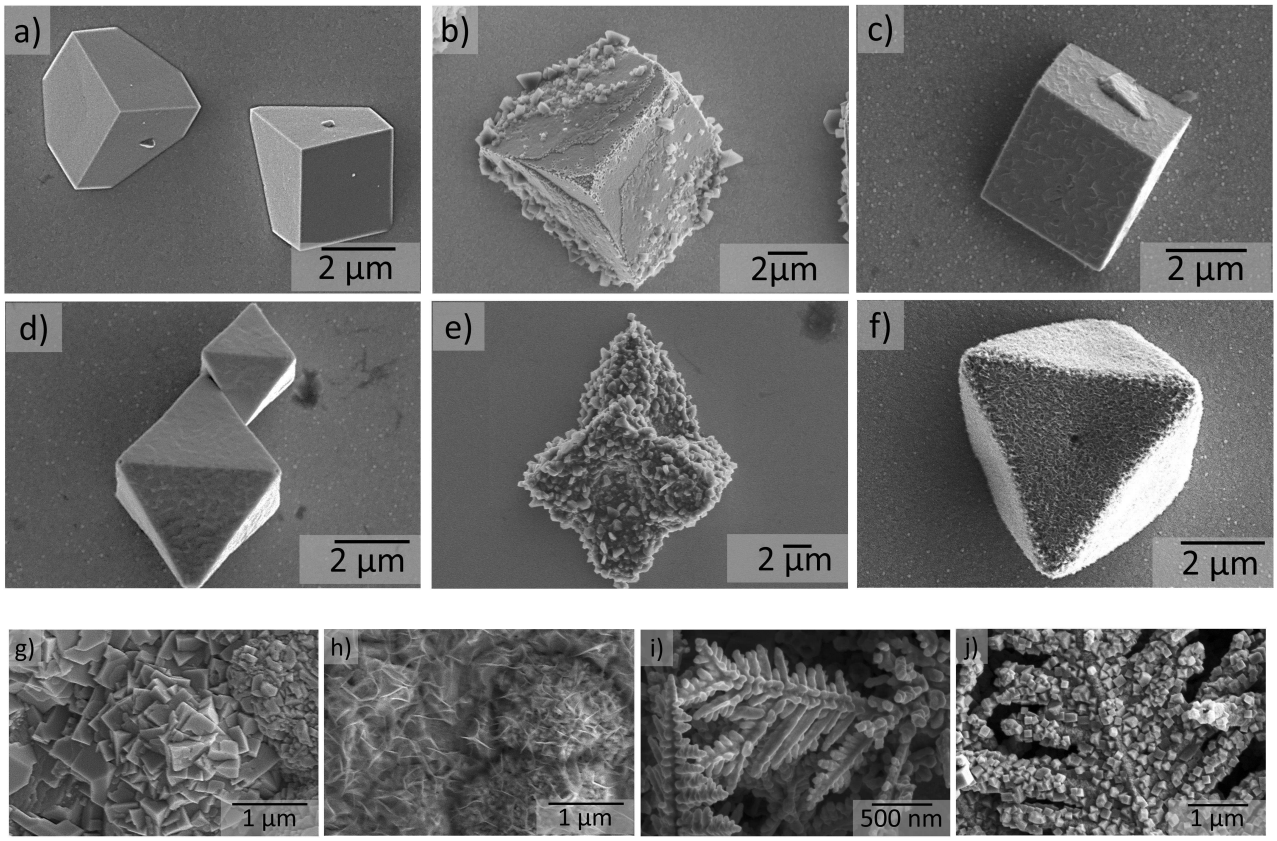

Figure 3. a–c) SEM images of Cu_2O cubes with exposed [100] planes a) before and b, c) after electrochemical conversion into either b) $Cu_3(BTC)_2$ or c) Cu(TCPP). d–f) Cu_2O octahedra with exposed [111] planes d) before and e, f) after electrochemical conversion into either e) $Cu_3(BTC)_2$ or f) Cu(TCPP). g–h) SEM images of Cu_2O dendrites g) before and h) after electrochemical conversion into Cu(TCPP). i–j) SEM images of Cu dendrites i) before and j) after electrochemical conversion into $Cu_3(BTC)_2$.

The use of additives in the electrochemical synthesis of the Cu_2O octahedra, and of the Cu_2O and Cu dendrites, allows the growth of less favorable crystallographic planes, overcoming thermodynamic (octahedra) or kinetic (dendrites) barriers.[36,37,41–47] These more unfavorable exposed planes dissolve faster by the applied bias, so more Cu^{2+} ions are available for the MOF conversion, reacting more efficiently with the organic linker in the electrolyte during the partial MOF conversion though anodic oxidation.

On all the presented Cu_2O microstructures, both $Cu_3(BTC)_2$ and Cu(TCPP) MOF showed a conformal coating after the proposed partial conversion, as shown in Figure 3. Additionally, using the obtained SEM images and the imaging software Image J, it was possible to roughly estimate a theorical and an empirical increase in size of the Cu_2O microcubes with exposed [100] planes of 38,7% for the $Cu_2O@Cu_3(BTC)_2$ and a 68,9% increase for the $Cu_2O@Cu(TCPP)$, as shown in the supporting information Figures S.12 and S.13, respectively. This increase was expected, due to the deposition of the Cu-based MOFs which are porous materials with an open pore structure.

XRD and Raman spectroscopy were also used to characterize the synthesized Cu_2O microstructures before and after their partial electrochemical MOF conversion. Unfortunately, there was no difference observed between the XRD patterns of the samples measured before and after the MOF conversion, which is due to the small amount of Cu-based MOF on the microstructures' surface (Supporting information, Figures S.14 and S.15). Therefore, Raman spectroscopy was employed as a structural fingerprint to precisely determine the chemical structure of the coating formed on the Cu_2O microstructures (Figure 4 and Supporting Information, Figure S.16).

As a general example, Figure 4a displays the obtained Raman spectra for the octahedral Cu_2O microstructures with exposed [111] planes, which visualize the difference between the initial Cu_2O octahedra and the prominent peaks of both obtained Cu-based MOF coatings. And in Figure 4b, the Raman spectra of the Cu_2O dendrites are shown, because they exhibit the most intense and prominent peaks belonging to Cu(TCPP) compared to all other microstructures (Supporting information, Figure S.16).

More specifically, in Figure 4a and 4b, the characteristic peaks of the bare Cu_2O are clearly visible in the region below 750 cm^{-1} in both Raman spectra (red curves). Additionally, in Figure 4a, the characteristic peaks of the $Cu_3(BTC)_2$ (green curve) can be observed in the region from 700 to 1100 cm^{-1}, and all peaks marked with an asterisk (*) were reported at the same Raman shift position for a $Cu_3(BTC)_2$ powder sample by Todaro et al.[70] Furthermore, the characteristic and most intense peaks

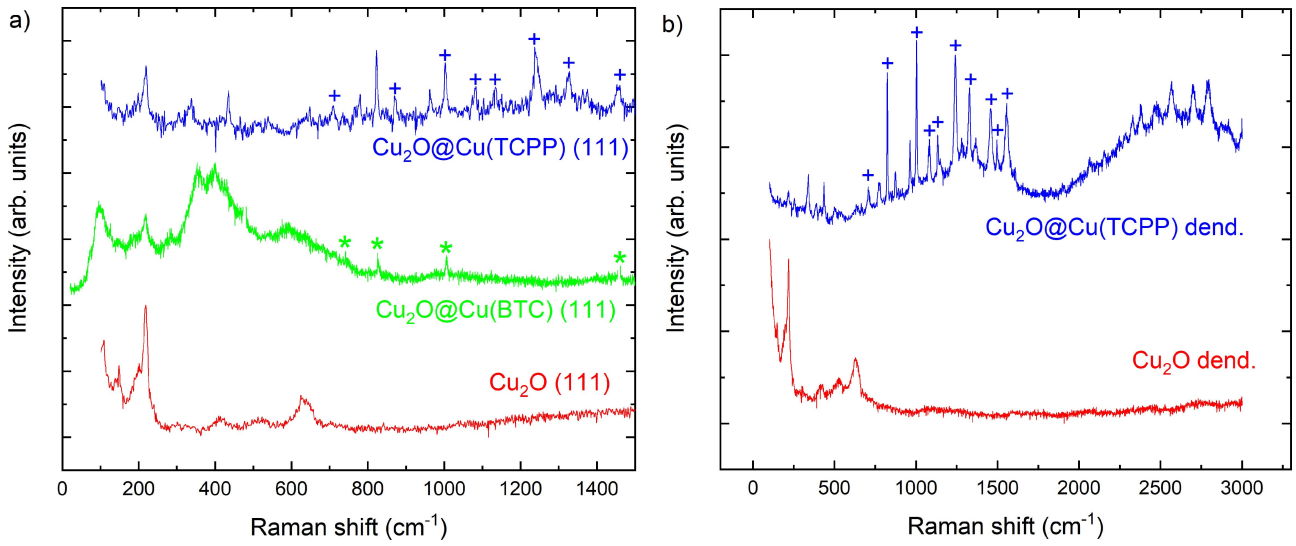

Figure 4. a) Raman spectra of octahedral Cu_2O microstructures on ITO substrates before (red curve) and after pulsed electrochemical conversion to core-shell $Cu_2O@Cu_3(BTC)_2$ (green curve) and core-shell $Cu_2O@Cu(TCPP)$ (blue curve) microstructures. b) Raman spectra of dendritic Cu_2O microstructures on ITO substrates before (red curve) and after (blue curve) pulsed electrochemical conversion to core-shell $Cu_2O@Cu(TCPP)$ microstructures at 25 °C.

of Cu(TCPP) (blue curves in Figure 4a and 4b) can be found in a wider region with a Raman shift between 750 cm^{-1} and 1750 cm^{-1} in both graphs, where the peaks marked with a plus (+) were reported at the same Raman shift position for a Cu(TCPP) powder sample by Sun et al.[71]

UV–vis spectroscopy can provide essential information about the optical properties of photoactive materials. Also, this characterization technique is particularly suitable for the observation of excited states. The prepared core-shell Cu_2O@CuTCPP and bare Cu_2O microstructures were therefore also characterized under UV and visible light irradiation, with the incoming beam approaching the sample first through the glass, followed by the ITO coating, to finally interact with the microstructures. This configuration was chosen to avoid that the absorption of the glass substrate interferes with the beam (UV light) after its interaction with the microstructures. In Figure 5, the absorbance of the as-synthesized bare Cu_2O dendrites (in red) is presented and compared with the as-synthesized core-shell $Cu_2O@Cu(TCPP)$ microstructures (in blue).

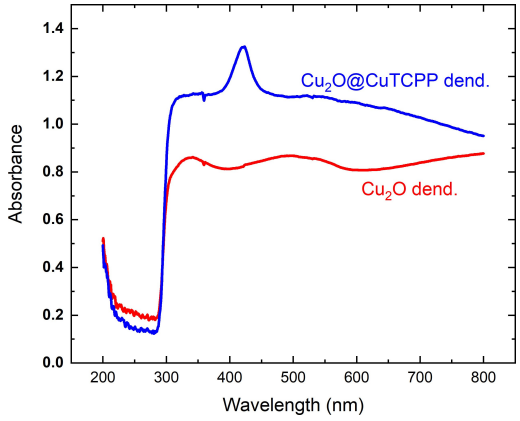

Figure 5. UV–vis absorbance spectra obtained from dendritic Cu_2O microstructures on ITO substrates before (red) and after (blue) their pulsed partial electrochemical conversion to core-shell $Cu_2O@Cu(TCPP)$ dendrites at 25 °C.

Figure 5 shows that, in general, the core-shell $Cu_2O@Cu(TCPP)$ dendrites absorb more light than the bare Cu_2O dendrites under visible and near-infrared light irradiation. The region between 400 nm and 450 nm presents a prominent peak in the absorbance of the core-shell $Cu_2O@Cu(TCPP)$ microstructures, which was also found for the other $Cu_2O@Cu$-(TCPP) microstructures (i.e. the cubes and the octahedra), as shown in the supporting information, Figure S.17. This peak was also reported by Xu et al.,[54] Rahimi et al.,[57] La et al.[58] and Zhuang et al.[73] at the same position for the pure Cu(TCPP) MOF as a powder, a thin film as well as for composites and hybrid materials.

The variation of the obtained UV–vis absorption spectra of the Cu_2O cubes and octahedra (Supporting information, Figure S.16) compared to the Cu_2O dendrites could be explained by an initial uneven distribution of the microstructures after their synthesis and the detachment of some microstructure from the surface after the partial electrochemical conversion. The dendrite sample has a complete coating, which contains a more uniform amount of Cu_2O and could improve its adhesion to the ITO substrate compared to the other two microstructures, so it is assumed that the dendrite microstructures could have a lower probability of detachment after the partial electrochemical MOF conversion.

Finally, it should be mentioned that Schäfer et al.[18] reported, that the presence of Cu_2O (or the possibility to form Cu_2O as an intermediate) is required to electrochemically synthesize $Cu_3(BTC)_2$. In this study, we have used both Cu thin films and Cu or Cu_2O microstructures as substrates, and showed that the synthesis of both $Cu_3(BTC)_2$ and Cu(TCPP) was possible on all of the investigated substrates. A possible explanation for this is the spontaneous formation of a Cu_2O layer on both Cu electrodes (the Cu thin films and Cu dendrites) after being

exposed to atmospheric oxygen, which makes the electrochemical MOF synthesis possible. This is also in agreement with two studies from Caddeo et al.[35,74]

Conclusions

This study presents the electrochemical synthesis and characterization of both Cu and Cu_2O microstructures and their conversion to either $Cu@Cu_3(BTC)_2$ or $Cu_2O@Cu(TCPP)$ via anodic dissolution. The bare Cu and Cu_2O microstructures, as well as the core-shell $Cu@Cu_3(BTC)_2$ and $Cu_2O@Cu(TCPP)$ microstructures were directly synthesized on ITO substrates. Initially, the Cu thin films were sputtered and the selected Cu-based microstructures (cubic Cu_2O with exposed [100] planes, octahedral Cu_2O with exposed [111] planes, Cu dendrites and Cu_2O dendrites), were electrochemically synthesized following the reported literature.[36,37] Then, these microstructures were used as substrates and only Cu source in the partial electrochemical conversion to either $Cu_3(BTC)_2$ or Cu(TCPP) using anodic dissolution. A successful synthesis depends on a low Cu^{2+} mobility away from the substrate surface and a strong adhesion of the formed crystals.

The combined use of photoactive Cu-based core-shell Cu@MOF and Cu_2O@MOF microstructures and ordered assemblies is a promising approach for microelectrodes and heterogeneous catalysis.

Experimental Section

Square 25 mm by 25 mm ITO glass electrodes (10 Ohm/sq, Präzisions Glas & Optik GmbH) were cleaned by immersion into 5 mL acetone (Acetone ≥ 99,5 % Roth) and 5 mL ethanol (Ethanol 99 % denatured, Chemsolute® Th. Geyer) for up to 5 minutes in each solvent using an ultrasonic bath. Then, the cleaned ITO substrates were used as working electrodes and immersed into different $Cu(NO_3)_2$ electrolytes to deposit the desired Cu_2O microstructures (cubes, octahedra or dendrites) adapting the reported literature..[36,37] All electrochemical experiments were done in a three-electrode setup with an ITO glass as the working electrode, a Pt mesh as the counter electrode and a saturated Ag/AgCl reference electrode using a PGSTAT 302N Autolab potentiostat with Nova 2.1 as the software suite, unless otherwise specified.

The Cu thin films were prepared by sputtering in an inert argon atmosphere with an adhesive intermediate layer of 20 nm of titanium followed by 70 nm of copper without interrupting the vacuum inside the chamber. A Leica EM ACE 600 – Double Sputter Coater was used to deposit the Cu thin films on the selected substrates. Afterward, the substrates were exposed to atmospheric conditions before MOF conversion.

The Cu_2O microcubes with [100] exposed planes were electrochemically synthesized following the report by Siegfried et al.[46] In short, an aqueous solution containing 0.02 M $Cu(NO)_3$ (Copper (II) nitrate trihydrate, 99–104 %, Honeywell Fluka) was prepared with its pH carefully adjusted to 4.1 at room temperature (approximately 23 °C) using HNO_3 (Nitric acid 65 %, Roth) or NaOH (0.1 M Sodium hydroxide 99.99 %, Sigma–Aldrich) before electrodeposition. Then, the cleaned ITO electrodes were immersed into this solution at 60 °C without any stirring and a potential of −0.02 V versus the reference electrode was applied for 300 s.

The Cu_2O octahedra with [111] planes exposed to the surface were electrochemically synthesized following Siegfried et al.[37] In short, an aqueous solution containing 0.02 M $Cu(NO)_3$, 0.17 M SDS (sodium dodecyl sulfate ACS reagent, ≥ 99.0 %, Sigma–Aldrich) was prepared. The pH of the solution was carefully adjusted to 4.1 using HNO_3 or NaOH at room temperature (approximately 23 °C) before adding SDS to the solution. Then, the cleaned ITO electrodes were immersed in this solution at 60 °C without any stirring and a pulsed electrochemical reduction was applied with an initial current density of $-0.18\ mA\,cm^{-2}$ versus the reference electrode for 0.1 s, and a resting current density of $0.0\ mA\,cm^{-2}$ versus the reference electrode for 0.9 s. These two pulses were repeated 1800 times, so the net deposition time was 3 min and the total deposition time was 30 min.

The Cu_2O dendrites were electrochemically synthesized following the conditions reported by McShane et al.[36] In short, a 0.08 M acetic acid buffer solution (Acetic acid 100 %, Roth) was prepared beforehand with a pH of 4.9 accurately adjusted at room temperature (approximately 23 °C) using NaOH. The clean ITO electrodes were immersed into an aqueous solution containing 0.02 M $Cu(CH_3COO)_2$ (Copper (II) acetate monohydrate, ACS, 98.0–102.0 %, Alfa Aesar) at 70 °C without any stirring. Then, a potential of −0.02 V versus the reference electrode was applied for 300 s.

The Cu dendrites were electrochemically synthesized following the conditions reported by Qiu et al.,[75] where the cleaned ITO substrates were completely immersed into an aqueous solution containing 0.1 M $CuCl_2$ (Copper(II) chloride dihydrate, 99 %, p.a., Carl Roth) and 0.1 M Na_2SO_4 (Sodium sulphate, 99 %, p.a., ACS, ISO anhydrous, powder, Carl Roth) at 25 °C without any stirring. A constant potential of −0.6 V versus the saturated Ag/AgCl reference electrode was applied for 300 s.

Afterwards, these Cu-based films and microstructures were exposed to an electrochemical MOF conversion to form either a BTC or a TCPP MOF coating on the microstructures' surface, using a pulsed potential profile. The first step was 2 V for 0.5 seconds, and the second step was 0 V for 0.5 seconds. This pulsed oxidation was repeated 120 times to avoid a complete conversion or detachment of the Cu_2O microstructures. The optimized electrolyte was prepared in a 75 % V/V ethanol-water mixture (Ethanol absolute p.a., ACS, Ph.Eur., USP. Chemsolute® Th. Geyer) at 25 °C without agitation, selecting the organic linker and the concentration of TEA (Triethylamine 99 %. Alfa Aesar), according to the desired MOF. It was either 5.8 mM of BTC (1,3,5-Benzenetricarboxylic acid 98 %, Alfa Aesar) and 17.4 mM TEA for the $Cu_3(BTC)_2$ MOF, or 5.8 mM TCPP (4,4',4'',4'''-(Porphine-5,10,15,20-tetrayl)tetrakis(benzoic acid) Dye content 98 %, Strem Chemicals, Inc.) and 23.2 mM TEA for the Cu(TCPP) MOF. The TEA was used to deprotonate the TCPP, as reported by Ji et al.,[14] making the controlled synthesis of the MOF via electrochemical oxidation possible. The concentration of TEA depends on the number of protons of the selected carboxylic acid, i.e. for BTC with its three protons, the concentration of TEA was 17.4 mM, while for TCPP with its four protons, the TEA concentration was 23.2 mM.

Subsequently, the bare Cu-based electrodes and obtained core-shell hybrid materials were characterized via SEM, XRD, Raman spectroscopy and UV–vis spectroscopy. The SEM characterization was done using a FEI Versa 3D dual beam system SEM using an accelerating voltage between 4–5 kV, an electron current between 20–25 pA, a working distance of 10 mm and an ICE detector. The XRD characterization was done using a Bruker D8 Advanced Bragg-Brentano X-ray Powder Diffractometer with a Cu radiation beam.

The measurements started at 5° and were stopped at 55°, with a step size of 0.0144°, a total of 3465 steps and 1 s per step. The Raman spectra were recorded using an InVia Raman spectrometer (Renishaw), which is connected to an optical microscope equipped with an XY stage (Prior Scientific) and an MS-10 stage controller (Renishaw), providing a position resolution of 0.5 μm. The laser excitation was performed at 532 nm with a grating of 1800 l mm^{-1}. Long working distance objectives (Leica, Wetzlar, Germany) were used with a magnification of 50×. Before use, the Raman spectrometer was calibrated to the 520.4 cm^{-1} peak of a silicon reference. The UV–vis characterization was done using a Shimadzu UV-2102 PC UV–vis Scanning spectrophotometer using the UV-2002/3102PC software version 3.0. The measurement was performed in transmission mode, the ordinate was 0 minimum and 2500 maximum, the wavelength varied between 800 and 200 nm, the scan speed was medium and the scan step was 2.0 nm, with an automatic scan interval.

Supporting Information

The authors have cited additional references within the Supporting Information.[23,76]

Acknowledgements

Financial support from the BMBF (grant Nr. FKZ 03Z22HN11) is gratefully acknowledged. Open Access funding enabled and organized by Projekt DEAL.

Conflict of Interests

The authors declare no conflict of interest.

Data Availability Statement

The data that support the findings of this study are available from the corresponding author upon reasonable request.

Keywords: Copper · electrochemical synthesis · metal-organic frameworks · microstructures · surfaces

[1] P. Falcaro, R. Ricco, C. M. Doherty, K. Liang, A. J. Hill, M. J. Styles, *Chem. Soc. Rev.* **2014**, *43*, 5513–5560.
[2] H. Li, M. Eddaoudi, M. O'Keeffe, O. M. Yaghi, *Nature* **1999**, *402*, 276–279.
[3] J. Liu, C. Wöll, *Chem. Soc. Rev.* **2017**, *46*, 5730–5770.
[4] A. Bétard, R. A. Fischer, *Chem. Rev.* **2012**, *112*, 1055–1083.
[5] J. Lei, R. Qian, P. Ling, L. Cui, H. Ju, *TrAC Trends Anal. Chem.* **2014**, *58*, 71–78.
[6] B. Li, M. Chrzanowski, Y. Zhang, S. Ma, *Coord. Chem. Rev.* **2016**, *307*, 106–129.
[7] R. J. Kuppler, D. J. Timmons, Q.-R. Fang, J.-R. Li, T. A. Makal, M. D. Young, D. Yuan, D. Zhao, W. Zhuang, H.-C. Zhou, *Coord. Chem. Rev.* **2009**, *253*, 3042–3066.
[8] C. Pettinari, F. Marchetti, N. Mosca, G. Tosi, A. Drozdov, *Polym. Int.* **2017**, *66*, 731–744.
[9] A. U. Czaja, N. Trukhan, U. Müller, *Chem. Soc. Rev.* **2009**, *38*, 1284–1293.
[10] H. Wang, Q.-L. Zhu, R. Zou, Q. Xu, *Chem* **2017**, *2*, 52–80.
[11] P. Kumar, A. Deep, K.-H. Kim, *TrAC Trends Anal. Chem.* **2015**, *73*, 39–53.
[12] H. R. Moon, D.-W. Lim, M. P. Suh, *Chem. Soc. Rev.* **2013**, *42*, 1807–1824.
[13] M. Müller, S. Turner, O. I. Lebedev, Y. Wang, G. van Tendeloo, R. A. Fischer, *Eur. J. Inorg. Chem.* **2011**, *2011*, 1876–1887.
[14] H. Ji, S. Hwang, K. Kim, C. Kim, N. C. Jeong, *ACS Appl. Mater. Interfaces* **2016**, *8*, 32414–32420.
[15] J.-L. Zhuang, A. Terfort, C. Wöll, *Coord. Chem. Rev.* **2016**, *307*, 391–424.
[16] R. Makiura, *Coord. Chem. Rev.* **2022**, *469*, 214650.
[17] R. Ranjan, M. Tsapatsis, *Chem. Mater.* **2009**, *21*, 4920–4924.
[18] P. Schäfer, M. A. Van Der Veen, K. F. Domke, *Chem. Commun.* **2016**, *52*, 4722–4725.
[19] H. M. Yang, X. L. Song, T. L. Yang, Z. H. Liang, C. M. Fan, X. G. Hao, *RSC Adv.* **2014**, *4*, 15720–15726.
[20] B. Van de Voorde, R. Ameloot, I. Stassen, M. Everaert, D. De Vos, J.-C. Tan, *J Mater Chem C Mater* **2013**, *1*, 7716–7724.
[21] P. Schäfer, Electrochemical Growth of CuBTC: Improving the Synthesis Toolkit through Mechanisticunderstanding, Doctoral dissertation, Johannes Gutenberg-Universität, **2017**.
[22] X. Zhang, K. Wan, P. Subramanian, M. Xu, J. Luo, J. Fransaer, *J Mater Chem A Mater* **2020**, *8*, 7569–7587.
[23] N. Campagnol, T. R. C. Van Assche, M. Li, L. Stappers, M. Dinca, J. F. M. Denayer, K. Binnemans, D. E. De Vos, J. Fransaer, *J Mater Chem A Mater* **2016**, *4*, 3914–3925.
[24] T. R. C. Van Assche, G. Desmet, R. Ameloot, D. E. De Vos, H. Terryn, J. F. M. Denayer, *Microporous Mesoporous Mater.* **2012**, *158*, 209–213.
[25] W.-J. Li, M. Tu, R. Cao, R. A. Fischer, *J Mater Chem A Mater* **2016**, *4*, 12356–12369.
[26] A. Martinez Joaristi, J. Juan-Alcañiz, P. Serra-Crespo, F. Kapteijn, J. Gascon, *Cryst. Growth Des.* **2012**, *12*, 3489–3498.
[27] T. R. C. Van Assche, N. Campagnol, T. Muselle, H. Terryn, J. Fransaer, J. F. M. Denayer, *Microporous Mesoporous Mater.* **2016**, *224*, 302–310.
[28] W. J. Li, M. Tu, R. Cao, R. A. Fischer, *J Mater Chem A Mater* **2016**, *4*, 12356–12369.
[29] A. Martinez Joaristi, J. Juan-Alcañiz, P. Serra-Crespo, F. Kapteijn, J. Gascon, A. M. Joaristi, J. Juan-Alcan, P. Serra-Crespo, F. Kapteijn, J. Gascon, *Cryst. Growth Des.* **2012**, *12*, 3489–3498.
[30] N. Campagnol, T. Van Assche, T. Boudewijns, J. Denayer, K. Binnemans, D. De Vos, J. Fransaer, *J Mater Chem A Mater* **2013**, *1*, 5827.
[31] J. L. Hauser, M. Tso, K. Fitchmun, S. R. J. Oliver, *Cryst. Growth Des.* **2019**, *19*, 2358–2365.
[32] U. Mueller, M. Schubert, F. Teich, H. Puetter, K. Schierle-Arndt, J. Pastré, *J. Mater. Chem.* **2006**, *16*, 626–636.
[33] V. M. Varsa, G. Nageswaran, *J Electrochem Soc* **2020**, *167*, 155527.
[34] J. L. Hauser, M. Tso, K. Fitchmun, S. R. J. Oliver, *Cryst. Growth Des.* **2019**, *19*, 2358–2365.
[35] F. Caddeo, R. Vogt, D. Weil, W. Sigle, M. E. Toimil-Molares, A. W. Maijenburg, *ACS Appl. Mater. Interfaces* **2019**, *11*, 25378–25387.
[36] C. M. McShane, K. S. Choi, *J. Am. Chem. Soc.* **2009**, *131*, 2561–2569.
[37] M. J. Siegfried, K. S. Choi, *Adv. Mater.* **2004**, *16*, 1743–1746.
[38] P. V. Kamat, *J. Phys. Chem. C* **2007**, *392*, 2834–2860.
[39] M. H. Tran, C. S. Yang, S. Yang, I. J. Kim, H. K. Jeong, *Chem. Phys. Lett.* **2014**, *608*, 207–212.
[40] H. Ma, P. Gao, P. Qian, Y. Su, *J. Phys. Chem. C* **2020**, *124*, 3403–3409.
[41] K.-S. Choi, *Dalton transactions (Cambridge, England: 2008)* **2008**, *40*, 5432–5438.
[42] M. J. Siegfried, K. S. Choi, *Angew. Chem. Int. Ed.* **2008**, *47*, 368–372.
[43] C. M. McShane, K.-S. Choi, *Phys. Chem. Chem. Phys.* **2012**, *14*, 6112.
[44] H. S. Jang, S. J. Kim, K. S. Choi, *Small* **2010**, *6*, 4–5.
[45] K.-S. Choi, H. S. Jang, C. M. Mcshane, C. G. Read, J. A. Seabold, K.-S. Choi, H. S. Jang, *MRS Bull.* **2010**, *35*, 753–760.
[46] M. J. Siegfried, K. S. Choi, *Angew. Chem. Int. Ed.* **2005**, *44*, 3218–3223.
[47] K. S. Choi, *J. Phys. Chem. Lett.* **2010**, *1*, 2244–2250.
[48] Y. Tan, E. M. P. Steinmiller, K. S. Choi, *Langmuir* **2005**, *21*, 9618–9624.
[49] M. Fytory, A. Mansour, W. M. A. El Rouby, A. A. Farghali, X. Zhang, F. Bier, M. Abdel-Hafiez, I. M. El-Sherbiny, *ACS Omega* **2023**, DOI 10.1021/acsomega.3c01385.
[50] H. Xia, J. Zhang, Z. Yang, S. Guo, S. Guo, Q. Xu, *Nano-Micro Lett.* **2017**, *9*, 43.
[51] Z. Cai, L. Deng, Y. Song, D. Li, L. Hong, Z. Shen, *Mater. Lett.* **2020**, *281*, 128616.
[52] R. A. Dodson, A. P. Kalenak, A. J. Matzger, *J. Am. Chem. Soc.* **2020**, *142*, 20806–20813.
[53] K. Koh, A. G. Wong-Foy, A. J. Matzger, *Chem. Commun.* **2009**, *41*, 6162–6164.
[54] G. Xu, T. Yamada, K. Otsubo, S. Sakaida, H. Kitagawa, *J. Am. Chem. Soc.* **2012**, *134*, 16524–16527.

[55] Y.-R. Lee, J. Kim, W.-S. Ahn, *Korean J. Chem. Eng.* **2013**, *30*, 1667–1680.
[56] Y. Sun, H.-C. Zhou, *Sci. Technol. Adv. Mater.* **2015**, *16*, 054202.
[57] R. Rahimi, S. Shariatinia, S. Zargari, M. Yaghoubi Berijani, A. Ghaffarinejad, Z. S. Shojaie, *RSC Adv.* **2015**, *5*, 46624–46631.
[58] D. D. La, H. P. N. Thi, Y. S. Kim, A. Rananaware, S. V. Bhosale, *Appl. Surf. Sci.* **2017**, *424*, 145–150.
[59] R. Evans, G. Dal Poggetto, M. Nilsson, G. A. Morris, *Anal. Chem.* **2018**, *90*, 3987–3994.
[60] G. Majano, J. Pérez-Ramírez, *Adv. Mater.* **2013**, *25*, 1052–1057.
[61] M. R. Lohe, S. Kaskel, L. H. Wee, J. A. Martens, N. Janssens, *J. Mater. Chem.* **2012**, *22*, 13742.
[62] J. Zhuang, D. Ceglarek, S. Pethuraj, A. Terfort, *Adv. Funct. Mater.* **2011**, *21*, 1442–1447.
[63] A. Ahmed, N. Hodgson, M. Barrow, R. Clowes, C. M. Robertson, A. Steiner, P. McKeown, D. Bradshaw, P. Myers, H. Zhang, *J Mater Chem A Mater* **2014**, *2*, 9085–9090.
[64] C. R. Groom, I. J. Bruno, M. P. Lightfoot, S. C. Ward, *Acta Crystallogr B Struct Sci Cryst Eng Mater* **2016**, *72*, 171–179.
[65] M. Morita, A. Yonezu, S. Kusaka, A. Hori, Y. Ma, R. Matsuda, *RSC Adv.* **2020**, *10*, 4710–4714.
[66] G. G. Hoffmann, *Raman Spectroscopy: Principles and Applications in Chemistry, Physics, Materials Science, and Biology/Günter G. Hoffmann*, Momentum Press, **2019**.
[67] S.-L. Zhang, *Raman Spectroscopy and Its Application in Nanostructures/ Shu-Lin Zhang*, **2012**.
[68] E. Smith, G. Dent, *Modern Raman Spectroscopy: A Practical Approach / Ewen Smith, Geoffrey Dent*, John Wiley & Sons Ltd, **2019**.
[69] P. Vandenabeele, *Practical Raman Spectroscopy: An Introduction*, **2013**.
[70] M. Todaro, A. Alessi, L. Sciortino, S. Agnello, M. Cannas, F. M. Gelardi, G. Buscarino, *Journal of Spectroscopy* **2016**, *2016*, 1–7.
[71] H. Sun, S. Cong, Z. Zheng, Z. Wang, Z. Chen, Z. Zhao, *J. Am. Chem. Soc.* **2019**, *141*, 870–878.
[72] N. Stock, S. Biswas, *Chem. Rev.* **2012**, *112*, 933–969.
[73] B. Zhuang, L. Xiangqing, R. Ge, S. Kang, L. Qin, G. Li, *Appl Catal A Gen* **2017**, *533*, 81–89.
[74] F. Caddeo, F. Himmelstein, B. Mahmoudi, A. M. Araújo-Cordero, D. Eberhart, H. Zhang, T. Lindenberg, A. Hähnel, C. Hagendorf, A. W. Maijenburg, *Sci. Rep.* **2023**, *13*, 13858.
[75] R. Qiu, H. G. Cha, H. B. Noh, Y. B. Shim, X. L. Zhang, R. Qiao, D. Zhang, Y. Il Kim, U. Pal, Y. S. Kang, *J. Phys. Chem. C* **2009**, *113*, 15891–15896.
[76] O. J. Rutt, G. R. Williams, S. J. Clarke, *Chem. Commun.* **2006**, *27*, 2869–2871.

Revised manuscript received: November 22, 2023
Accepted manuscript online: November 24, 2023
Version of record online: December 15, 2023